We are IntechOpen, the world's leading publisher of Open Access books Built by scientists, for scientists

4,800
Open access books available

122,000
International authors and editors

135M
Downloads

Our authors are among the

154
Countries delivered to

TOP 1%
most cited scientists

12.2%
Contributors from top 500 universities

WEB OF SCIENCE™

Selection of our books indexed in the Book Citation Index in Web of Science™ Core Collection (BKCI)

Interested in publishing with us?
Contact book.department@intechopen.com

Numbers displayed above are based on latest data collected.
For more information visit www.intechopen.com

3

MEMS Microfluidics for Lab-on-a-Chip Applications

Nazmul Islam and Saief Sayed
MEMS/NEMS Lab, The University of Texas at Brownsville
USA

1. Introduction

Micro-/Nano- fluid devices are becoming more prevalent, both in commercial applications and in scientific inquiry. Microfluidics, a branch of MEMS (Micro-Electro-Mechanical Systems) is key enabling factor in the miniaturization and integration of multiple functionalities for chemical analysis and synthesis in handheld microdevices, which require efficient methods for manipulating ultra small volumes of liquid as well as the contents in the fluid within the fluid networks. For biomedical applications, microfluidic chip arrays are being used to identify multiple bioparticles [1]. Recent developments in micro-fabrication technologies enabled different types of microfluidic functions such as micro-pumps [2, 3], micro-mixers [4], particle concentrator [5, 6], and various s types of injection systems (nano-needles). At the very beginning of microfluidics, people thought that microfluidic devices could just be a miniaturized version of macro- fluidic devices. The technological advancement on microfluidic systems has proven that the problem is far more complicated than scaling down a device geometrically. Therefore, a better understanding of the micro/nano scale properties is in order.

A dominant difference of microfluidic devices from their macro-scale counterparts is the increased surface/volume ratio, hence dominant surface force effects/friction. Micro channel needs high pressure for pressure driven flow to produce sufficient flow rate. The formula below relates the applied pressure with the conduit radius for a constant flow rate.

$$\Delta P = \frac{8\mu LQ}{\pi a^4} \qquad \mu : \text{viscosity}; \quad a : \text{conduit radius}$$

Every time we try to reduce the conduit radius into half, we need to have sixteen times of larger pressure to sustain the same flow rate. So at microscale, surface forces start to dominate due to the large surface/volume ratio. Therefore electroosmosis (as a type of surface forces) becomes the prime candidates for fluidic manipulation at micro scale. Direct Current Electroosmosis (DCEO) has a long history of being applied in miniaturized biochemical devices. However, DCEO has many undesirable effects, such as high voltage operation, electrolysis and resulting bubble generation, and pH gradient. In this chapter, we examined a new type of EO phenomena, ACEO (Alternating Current Electroosmosis), and how it can be employed to integrate with the microcantilever particle trapping.

2. MEMS microfluidics: Past, present and future

Microfluidics is an interdisciplinary area that focuses on the miniaturization of fluid-handling systems. The concept of complete lab-on-a-chip devices or micro-total analysis systems (μ-TAS), has recently generated great interest in a variety of industries, where transport and processes (including mixing, reaction, separation, and manipulation of chemicals and particles) are being applied on much smaller scales than traditional engineering technologies [7, 8]. This interest has led to tremendous growth in microfluidic technologies over the past decade.

A functional microfluidic chip should be able to realize certain functions, such as transporting, mixing (with reactants), sample treatment (concentrating, sorting). Figure 1 gives an example of a generic microfluidic chip. Unlike the microelectronics industry, where the current emphasis is on reducing the size of transistors, the field of microfluidics is focusing on investigating new fluid phenomenon at micro/nano-scale with more sophisticated fluid-handling capabilities. One of the promising types of micropumps is driven by electroosmosis (EO). EO pumps are purely driven by electric fields and have no moving parts. The central concept is utilizing the surface force. As the surface to volume ratio of the microchannel is high, the dominant surface force is a good choice for pumping the liquid in microchannel.

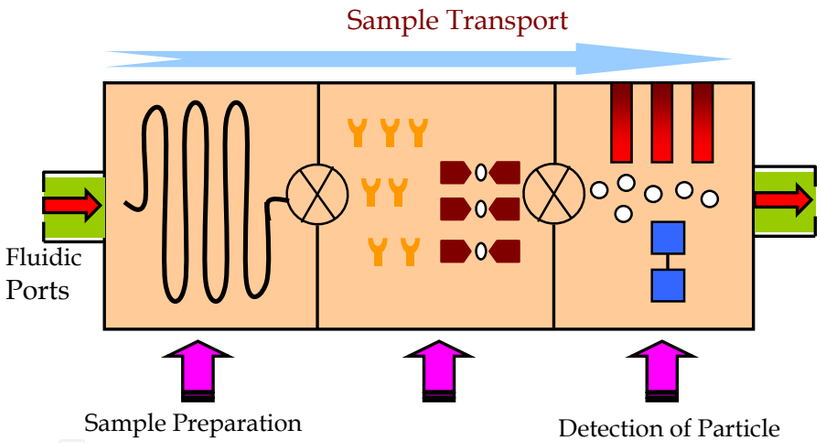

Fig. 1. A Generic Microfluidic Chip with the sample preparation, selection and detection of bio/nano/micro-particles.

As mentioned before, the field of microfluidics has far more complexity than people first expected. The dominant/efficient mechanism to manipulate fluid or biochemical samples will change with sample conductivity, pH value, and sample sizes. Also, we need to be concerned with side effects from those actuation mechanisms. So microfluidic industry did not develop in a similar way as the microelectronics industry. Lab-on-a-chip (LOC) devices have shown commercial success in biological applications such as electrophoretic separations and DNA sequencing, where DC electrokinetics or DC electric field is used to manipulate fluid/particles (here surface force is used versus pressure driven). However, because of its operation with high voltage, there are obstacles to extend DC electrokinetics to more fluidic functions. On the other hand, AC electrokinetics has important potentials in the field of life science. With the capability to manipulate particle and fluid motion at

the microscale with low voltage, it meshes well with the requirements of lab-on-a-chip systems.
In this chapter a combination of sample transportation and particle detection in a microfluidic chip. As shown in figure 1, we need to transport the sample, for which I have experimentally validate the biased ACEO micro-pumping. The developed micropump is operated with smaller AC voltage, which is compatible with the lab-on-a-chip. For particle detection as shown in figure 1, we need high effective techniques to detect micro/nano-scale particulate. We also have envisioned to develop the validation technique for particle trapping. That is the reason we have interface the microcantilever with our microfluidic device. The applications of this integration can greatly benefit the advancement of AC electrokinetics.

3. Electrokinetics

Electrokinetics is the combination of "electric" plus "kinetics". Generally speaking, electrokinetics is the motion of liquid or particle under the influence of electric field. According to Probstein [7], the electrokinetic effects have been first observed by F. F. Reuss in 1809 via experiments on porous clay diaphragms. He has shown that in capillary, fluid moves from anode to cathode in the presence of an external electric field. In the mid 19th century, Wiedemann repeated this experiment and described the fundamentals of electrokinetics. This was followed later by the seminal work of Helmholtz in 1879 on the electric double layer theory, which related the electrical and flow parameters for electrokinetic transport. DC electrokinetics, including electroosmosis and electrophoresis, has almost two hundreds years' history and has been rather thoroughly investigated. Electroosmosis is the fluid motion caused by the electrical force acting on the double layers next to a charge surface. The ions in a double layer are moved by a tangential electric field, giving rise to movement of the whole double layer along the surface, which in turn puts the bulk fluid into motion through the viscous interaction.
On the other hand, AC electrokinetics has been studied for just a few years. AC electrokinetics can be classified into three categories, dielectrophoresis (DEP), the electrothermal effect (ET) and ac electroosmosis (ACEO). DEP is the force acting on the particles due to the difference in polarizability between the particles and the fluid. The electrothermal effect refers to the fluid motion caused by the interaction of electric fields and gradients of conductivity and permittivity of the fluid through Joule heating. AC electroosmosis is the fluid motion induced by moving double layers. We will focus on the AC electroosmosis, while we will discuss the effects from other electrokinetic phenomena. Basically, AC electroosmosis (ACEO) works by the same principle as DC EO. However, in ACEO, the surface charges are induced by externally applied voltages, rather than naturally occurring charges in DCEO, and consequently hundreds of time stronger. As a result, ACEO can generate flow velocity of several hundreds microns per second with a couple of volts.
AC techniques are more favorable over DC ones for following reasons: (1) low operating voltage makes it superior in terms of device portability; (2) avoids electrolysis and the resulting bubble generation; (3) minimizes pH gradient; (4) miniaturization and integration with other devices on lab-chips. We have extended the scope of ACEO by including electrochemical reactions (i.e. Faradaic charging), and then developed a new ACEO technique—asymmetric polarization ACEO. Asymmetric polarization of electrodes is achieved by combining the DC bias into AC signals over electrode pairs. Biased ACEO breaks the reflection symmetry to produce net flow in a symmetric pair of electrode. This technique adds more flexibility to the faster manipulation of bio-particulate.

3.1 AC Electrokinetics

AC electrokinetics provides a means to effectively control and manipulate particles and fluids at micro-scale. Switching electric field of AC elctrokinetics can suppress the electrolysis and hence the change of pH value at electrodes, which is inevitable in dc electrokinetics. Different from DC EO which relies on naturally induced charges, ACEO induces surface charges by applying voltage, which can be hundreds of times higher lower voltage is required to generate sufficient flow velocity. Additionally small spacing of electrodes makes it possible to reach high electric field (E) with low applied voltage (V). AC electrokinetics can operate low voltages, which is suitable for lab-on-a-chip operation.

AC electrokinetics comprises of dielectrophoresis, the thermal effect and ac electroosmosis. Dielectrophoresis (DEP) is the response of particles to the applied electric fields, and the electrothermal effect and ac electroosmosis are fluid motion caused by AC fields. Ramos et al have provided a rather comprehensive review [9] on various forces acting on micro-size particles on microelectrode arrays when electrodes are energized with ac voltages over a wide range of frequency. In subsequent work, Ramos et al [10] presented a RC model describing the frequency dependence of ACEO flow velocity by capacitive charging of the electrodes. Recently, Bazant and Squires [25, 28] also presented that AC electrokinetic phenomena can also occur for conducting particles, which they termed as Induced charged Electroosmosis (ICEO). They also predict that the velocity will scale as E^2, where E is the applied electric field. Vortices will also occur around a spherical metal because of their geometry. Bhatt [5] also reported that electrohydrodynamic effect arising from the application of alternating electric fields to patterned electrode surfaces.

3.2 AC Electroosmosis

ACEO was first investigated using a pair of planar electrodes as shown in figure 2. In figure 2, a pair of electrodes is placed parallel in an electrolyte. The first half cycle of the applied signal is shown in figure 2(a). The double layer is produced on the electrode surface like dc electroosmosis. Therefore there is a nonzero tangential component of electric field acting on the double layer. The interaction of this tangential electric field with the surface charge creates the force according to the Coulomb's law. This force is along the electrode, which in turn puts the fluid in motion. In the half cycle of the applied AC signal, the sign of the surface potential becomes reversed, as shown in figure 2(b). The ions move accordingly, keeping the sign of the double layer opposite to the potential. At the same time, the electric field also reversed its direction. So in this case both surface charge polarity and the electric field direction changed. Subsequently, the force acting on the double layer is still the same direction as in the first half cycle, keeping the fluid motion unchanged.

AC electroosmosis is much more complicated than DC electroosmosis due to two reasons: 1) The applied signal is oscillating; 2) The surface charge and the tangential field are coupled. An excellent experiment and theoretical study of AC electroosmosis can be found in [9, 10, 38]. The governing equations for the fluid motion inside the double layer is represented by following equation coupled with the continuity equation.

$$\rho_m \frac{D\vec{u}}{Dt} = -\nabla p + \mu \nabla^2 \vec{u} + \rho \vec{E} \tag{1}$$

Neglecting the term on the left hand side of equation (1) leads to,

$$-\nabla p + \mu\nabla^2 \vec{u} + \rho \vec{E} = 0 \tag{2}$$

The fluid velocity can be obtained after substituting the charge density (ρ) and the electric field distribution into equation (2). The fluid velocity at the outer boundary of the double layer is given by,

$$\vec{u}_f = -\frac{\varepsilon}{4\mu} \Lambda \nabla_s \left(\left| \Delta V \right|^2 \right) \tag{3}$$

where Λ is a factor of the double layer structure, Δ_s represents a gradient across the surface, and ΔV is the potential drop across the double layer. According to the equation (3), fluid tends to move from higher electric field region to the lower electric field region. The fluid velocity at the electrode surface is,

$$u_s = \frac{1}{8} \frac{\varepsilon V_0 \Omega^2}{\mu s \left(1 + \Omega^2\right)^2} \tag{4}$$

where V_0 is the voltage amplitude and s is the distance from the electrode center. Ω is the nondimensional frequency,

$$\Omega = \omega \frac{\varepsilon}{\sigma} \frac{\pi}{2} \frac{s}{\lambda} \tag{5}$$

where ω is the angular frequency and λ is the debye length.
Equation (4) gives a bell-shaped velocity profile with respect to the frequency. At high and low frequencies the velocity approaches to zero. We experimentally verified this bell-shaped velocity profile in our research. Our research emphasizes on the charging processes of electrodes. By studying surface EO flows with respect to AC potential, we identified ACEO induced by electrochemical reactions (i.e. Faradaic charging), and we have developed a new ACEO technique — asymmetric polarization ACEO. Here we also explain the competition between the Faradaic and Capacitive charging process.

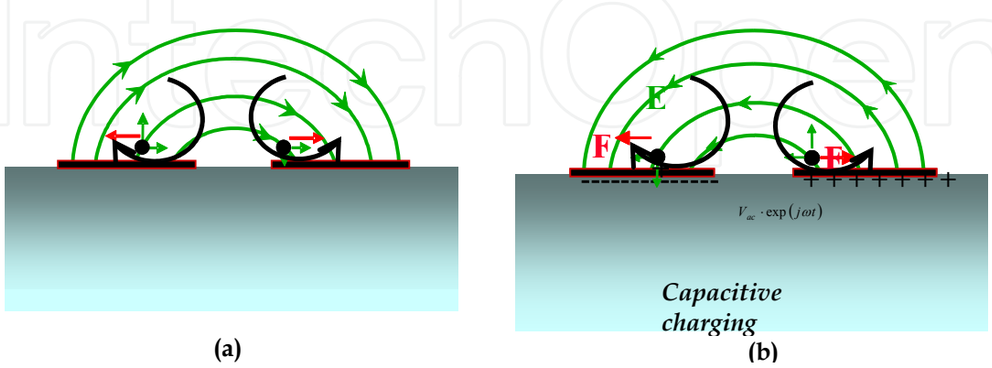

Fig. 2. ACEO fluid motion and induced charge at electrode surface. (a) during the half cycle when the left electrode has positive polarity; (b) during the next half cycle with opposite electrical polarity.

Faradaic charging generates co-ions from electrochemical reactions. When the electrode is positively charged, it goes through the reaction according to the Faradaic's law. On the other hand, capacitive charging attracts counter-ions from the electrolyte to screen the electrode potential. Our contribution in this field is that we have developed an "asymmetric polarization (A-P) ACEO" technique by adding a DC offset to the AC signal, and we used this A-P ACEO for trapping particles on the electrodes [11]. Asymmetric polarization of electrodes in a pair is achieved by combining the DC bias into AC signals over electrode pairs. For adding DC bias the reflection symmetry of electrode charging is broken, leading to asymmetric surface flow and net-flow. By adjusting the amplitude and frequency of AC signals, a variety of directed surface flows are produced on electrodes to manipulate and transport particles.
Capacitive charging and Faradaic charging coexist and compete for dominance when the electrodes are energized under biased conditions. The biased ACEO scheme is built on the fact that the two electrodes in a pair undergo the two distinct polarization processes. Biased AC EO is implemented by energizing electrode pairs with biased AC signals so that electrodes in a pair undergo polarizations different from each other. The advantage of such a scheme is twofold. First, it breaks the mirror symmetry of electric fields and, consequently, that of surface flows. If Faradaic charging occurs on one electrode while capacitive charging takes place on the other, then ions of the same sign populate the electrode surface and they migrate in the same direction under the influence of the electric fields. As a result, a unidirectional flow is produced at the electrode surface. So, non-uniform electric field has a good application in pumping action.

3.3 Fabrication of microfluidic devices

The processes developed for microelectronics, such as standard photolithographic methods, can be applied to silicon and glass substrates producing channel networks in two dimensions for sample transport, mixing, separation, and detection systems on a monolithic chip (Fig 1). A mask is made that has transparent and opaque regions that are patterned as a negative image of the desired channel layout. A UV-light source transfers the layout from the mask to the photoresist, which has been previously deposited on the substrate by spin-coating. The photoresist is then developed in a solvent that selectively removes either the exposed or the unexposed regions.
After developing the photoresist, it has a small amount of "hydrocarbon" material still on the wafer. If this is not removed it can affect the geomarty. Removing this very thin layer is something we call "descum". To descum we used an oxygen plasma generated in a parallel-plate etcher (Reactive Ion Etching – RIE). The oxygen plasma interacts with our undesirable hydrocarbon layer and burns it away. Then we deposit gold using the E-beam evaporator. As an adhesive layer we have used Cromium (Cr) between the gold and the wafer. After that photoresist is removed by lift-off process, and interdigitated electrode pattern is created for microfluidic experiment. Typical fabrication sequence is shown in the figure 3. Here we have shown the negative photolithography, where the image reversal is used.
Polymer based microfluidic devices are also getting much attention recent days. Polymer is resistant to chemicals and some are biocompatible for implantation by FDA [37]. PDMS has shown a number of advantages over other polymer materials (eg. SU-8, PMMA): PDMS microchips can be easily replicated and produced by rapid prototype approaches with low cost [31]. The excellent optical transparency of PDMS has been exploited to integrate different elements in the optical detection.

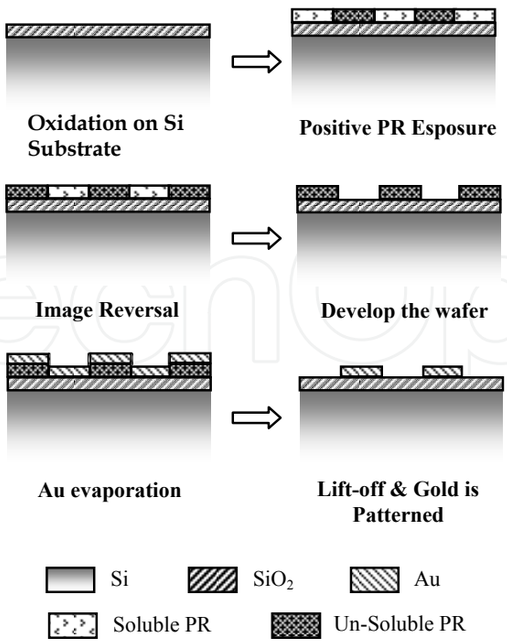

Fig. 3. Fabrication sequence for silicon, and glass microfluidic devices

For our experiments we have used PDMS to fabricate our microchannel for microfluidics particle trapping and micropumping. The first step of fabricating microchannel is to have the mold. We have fabricated the channel dimensions as low as 100 µm X 100 µm [cross-section]. Following is the steps of fabricating microchannel for our experiments.

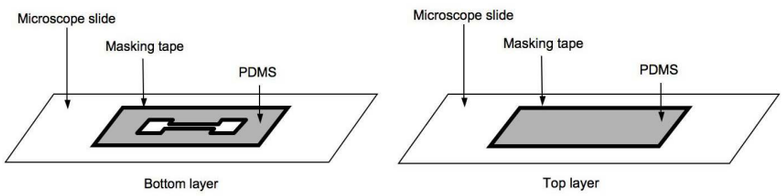

a. PDMS on two substrates to create a bottom layer and a top layer of the microchannel pump

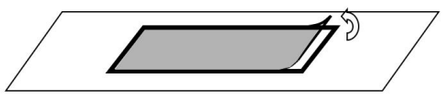

b. Top layer PDMS was peeled from the substrate after thermally cured

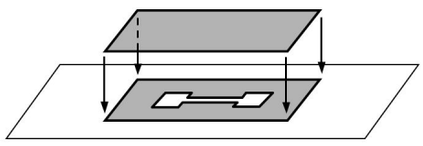

c. Top layer PDMS was placed on top of the patterned bottom layer

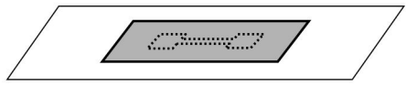

d. Top view of the sealed microchannel pump

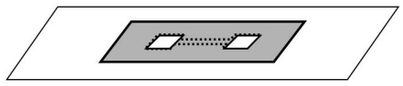

e. Two rectangular cuts were made for reservoirs

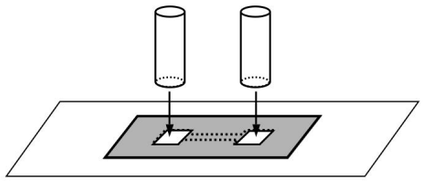

f. Integrating the reservoirs onto the pump

Fig. 4. Steps of fabricating microfluidic chamber

1. PDMS was prepared by thoroughly mixing the silicone Base and Curing Agent (SYLGARD 184 Silicone Elastomer Kit, Dow Corning, Midland, MI) at ratio 10:1 base:curing agent using a portable mixer. The mixture was then set in a small plastic container to reduce the air bubbles from the mixing process. This was done in approximately 30 minutes or until there were no visible bubbles. The PDMS was then poured onto two different glass substrates (microscope glass slides).
2. The first substrate functioned as the bottom layer, which was patterned using a piece of masking tape. The pattern defined the profile of the microfluidic pump. It contained a microchannel that connected two reservoirs at the end of the channel. The second substrate created the top layer, which would be used as the channel sealer. (See Figure 4a). Both substrates were thermally cured on a hot plate for 10 minutes at 150°C.
3. The PDMS for the top layer was then peeled from the glass substrate and was placed on top of the PDMS for the bottom layer. A careful placement was done to avoid any air gap between the two layers. Hence, to prevent a leak of the working liquid. (Figure 4-b, c, and d).
4. Two rectangular cuts were made on the top layer outlining the reservoir contours of the bottom layer. (Figure 4e).
5. Two reservoirs were made by cutting a glass pipette into two two-centimeter tubes. They were integrated on the pump using a 5-minute epoxy glue. (Figure 4f).

One of the most important advantages of PDMS is that it is easy to fabricate and allows a simple sealing with the planar substrates. However, PDMS has three significant problems in practical use.

- Dissolution or swelling by organic solvents.
- Absorption of chemical materials.
- Adhesion between PDMS and metal layer is not intact/perfect

To overcome these problems, we have coated PDMS with perfluoro amorphous polymer on the PDMS micro structures, which minimizes the problems of PDMS [36]. Perfluoro amorphous polymer (CYTOP, CTX-809A, Asahi Glass Company, Japan) is coated by spin coating on the PDMS structure. Since natural PDMS surface repels CYTOP, so we used O2 plasma pre-treatment on the surface before CYTOP coating. Our preliminary result shows

that CYTOP coating was achieved without any deformation of the micro structure. This polymer based substrate with CYTOP can be used in different biological, chemical and lab-on-a-chip (LOC) applications.

The need for innovative fabrication methods to integrate higher levels of functionality into microfluidic and lab-on-a-chip devices is growing almost as rapidly as the number of potential applications for these miniature devices. The ability to make fully-integrated, multi-level fluidic systems with functional valves, pumping systems, electrical and electronic components, and other microeletromechanical system (MEMS) components is essential in order for this relatively new field to reach its full potential.

3.4 Electric field analysis

We have used Comsol Multiphysics (formerly FEMLab) to simulate the electric field distribution above a pair of planar electrodes (160micron width and 40 micron separation between the electrodes, with infinitesimal thickness). As shown in Figure 5a, tangential electric fields change directions over one electrode, which indicates that two counter-rotating vortices exist on one electrode, as schematically drawn in Figure 5b, countering to one vortex reported in the litereature.

The fluid velocity on the electrode surface is given [5] as

$$u = -(\varepsilon / \eta)(\xi - \varphi_b)E_t \tag{6}$$

where ε is the permittivity, η is the viscosity of bulk solution, $(\xi - \varphi_b)$ is the difference of potential between the double layer and the bulk solution, Et is the tangential component of electrical field. According to Equation 6, the velocity on the surface of double layer is proportional to the tangential field and potential difference between the double layer and fluid, which corresponds to the normal component of electrical field. Therefore, normalized boundary conditions on both electrodes are given as, $u = -E_x E_y$.

To model the fluid motions, the 2D Incompressible Navier-Stokes module is used in FEMLAB. In this case, the hydrodynamic property in the chamber is given as density = 1000 $kg.m^{-1}$ and viscosity = 10^{-3} $kg.m^{-1}.sec$. The fluid velocity distribution is then obtained by solving Navier-Stokes equation with calculated field profile.

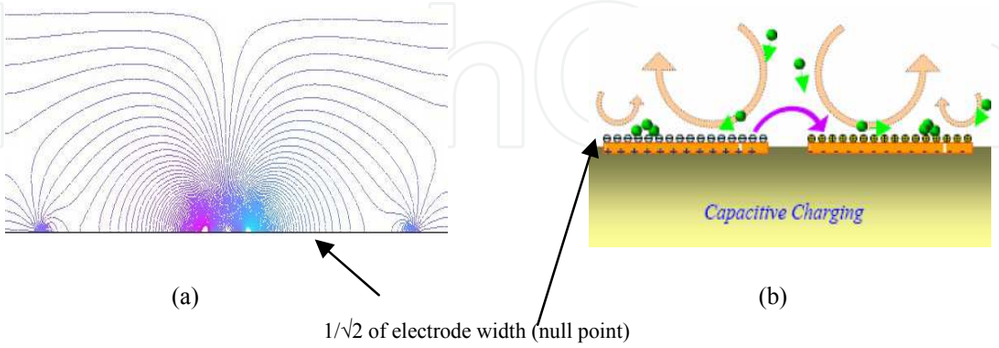

Fig. 5. (a) Comsol simulation for the Electric field distribution above a pair of planar electrodes with voltage of +1V & -1V in two electrodes (160/40micron). (b) Four counter-rotating vortices are formed above the electrodes due to changes in tangential electric fields, which facilitate particles aggregation on electrodes.

3.5 Impedance analysis for optimization

The charging and ion migration process at electrodes can be represented by an equivalent circuit element. To analyze the effect of ACEO, it is necessary to develop an RC equivalent circuit for the pair of electrodes. Figure 6(a) is the equivalent circuit for the planar electrode in an aqueous environment. There are two paths that the planar interdigitated electrodes are connected as shown in the figure. One path goes through Ccell, which stands for the direct dielectric coupling between electrodes and it jumps the dielectric coupling through the fluid, and the environment. The other path goes through the fluid, which can be treated as resistance since it obeys Ohm's law. It is in series with capacitance for double layer charging at the interface of electrolyte and electrode on both ends. Figure 6(b) is the simplified RC equivalent circuit model. At low frequency, the reactance from double layer capacitance is high. Thereby a large portion of voltage drop happens within the double layer, suitable for the ACEO phenomenon to take place. At high frequency, time is limited for double layers to form, consequently inducing a great amount of surface charge in the double layer.

So, for the high frequency case the reactance gets smaller and more voltage drop across the resistive bulk fluid. As there is little voltage drop, hence little surface charge on the electrode, so ACEO becomes negligible at high frequency. By using the equivalent circuit model we can theoretically analyze the frequency range for the ACEO mechanism.

$$Z_{\mathrm{mod}eled} = \left[j\frac{1}{2*pi*f*C_{cell}} \quad || \quad \left(R_{sol} + j\frac{1}{2*pi*f*C_{tot\_dl}} \right) \right] + 2R_{lead}$$

The values of the above mentioned components in the equivalent circuit can be extracted by impedance measurements. 5 mV_{rms} excitation level was used for impedance measurement. For 5 mV excitation level in can be very well assumed. In this condition faradaic charging will not take place, so we neglected the faradaic charging (Fig. 6b) for this analysis. The simplified equivalent circuit is shown in Fig 6(b). Following is the modeled impedance value,

$$Z_{\mathrm{mod}eled} = \left[j\frac{1}{2*pi*f*C_{cell}} \quad || \quad \left(R_{sol} + j\frac{1}{2*pi*f*C_{tot\_dl}} \right) \right] + 2R_{lead}$$

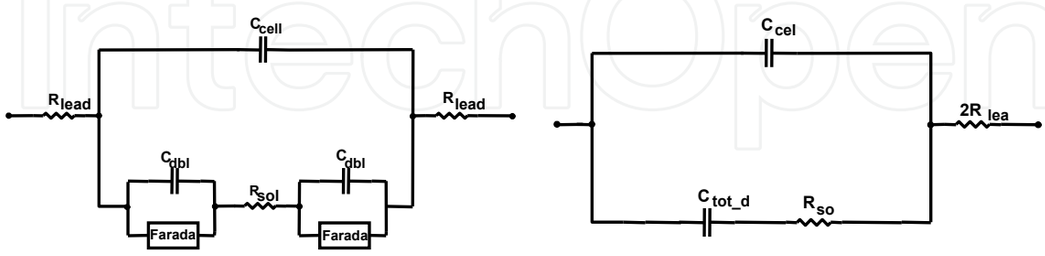

(a) (b)

Fig. 6. Equivalent impedance for interdigitated pattern; (a) RC equivalent circuit for planar electrode configuration; (b) Simplified RC equivalent circuit for the modeling.

C_{cell} and C_{dbl} can be extracted from the experimental plot. At smaller frequency the C_{dbl} is dominated and at higher frequency $C_{cell/dielectric}$ dominants. Our extracted parameters are,

C_{cell} = 305 pF; C_{dbl} = 28.85 nF; R_{lead} = 18 Ω; R_{sol} = 966.234 Ω. We put all these values to our $Z_{modeled}$ and compare the plot with the experimental impedance plot from the impedance analyzer. The two plots matched fairly, so we can conclude that our extracted modeled parameter is correct.

The impedance measurements have been done for two different situations, 1) the electrode pair in DI water, and 2) the electrode pair in the DI water seeded with particles. We use information from impedance measurement to optimize the operating condition (signal frequency, magnitude etc.) of ACEO. Impedance plot for the two different excitation levels are also compared in figure 7. As seen from the figure, for high excitation voltage the impedance goes down. This is because the charge, Q is constant in the double layer, and the double layer capacitance is inversely proportional to the applied oscillator voltage (Q=CV). That is the reason the impedance plot for the two different excitation levels are different.

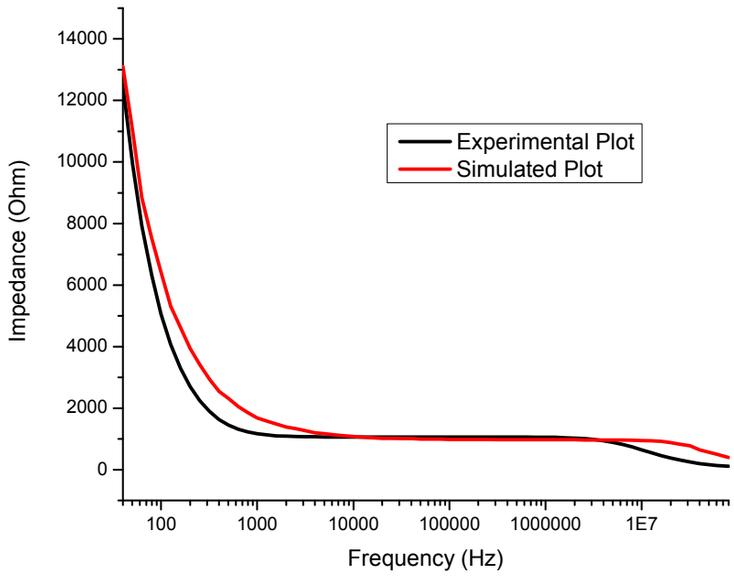

Fig. 7. Comparison of impedance plot between the experimental and the modeled data

Nyquist plot shows the frequency response for the linear system. Figure 8 shows the Nyquist plot for the equivalent circuit. The low frequency area of Nyquist plot denotes the double layer capacitive effect. Point "a" denotes the solution of resistance, which we extracted from figure 7 is 966.234 Ω. The graphical representation (figure 8) using a Nyquist plot represents the two parallel path of the microfluidic system, so that we can analyze the pre-dominant of the impedance in smaller and higher frequency range. The impedance analysis is very important to distinguish the effect of different electrokinetic forces.

From the figure 7 we also can see that the difference of the impedance with and without the particle is more in frequency below 1 KHz. So we adopted signal frequency range between 100 Hz to 1 kHz for particle trapping. The experiment was done at 500 mV_{rms} oscillation level. Same characteristics were obtained at 1 V_{rms}. Our goal is to determine a higher velocity electrode pattern with the polystyrene particle, so both experiments and calculation were performed to determine the optimum signal magnitude for these four sizes of electrode pair (160/40, 160/20, 80/40, 80/20).

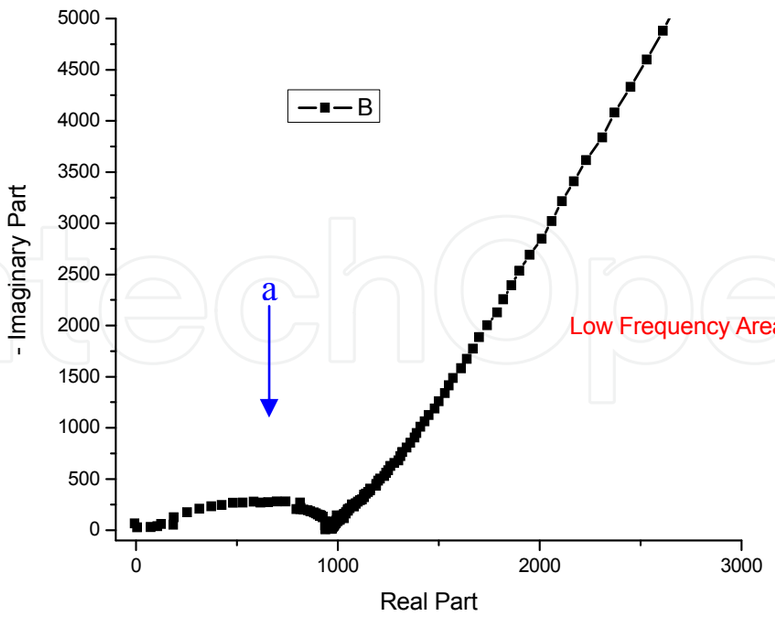

Fig. 8. Nyquist Plot for real vs Imaginary plot at 5mV Osc Level

4. Biased AC electroosmosis micropump

Micropump is critical to transport small amounts of fluid for many microfluidic applications, ranging from drug delivery, bio-fluid analysis, to microelectronics cooling. With the development of MEMS technology, micropumps have been designed and fabricated to integrate with lab-on-a-chip (LOC). Due to the large surface to volume ratio in microchannels, surface tension and viscous forces play an important role in the flow characteristics. So for micropumping action we need to choose the electroosmosis technique which benefits from the higher surface to volume ratio. For this reason electroosmotic action is suitable for miropumping action.

Electroosmotic (EO) pumping is the motion of bulk liquid caused by the application of an electric field to a channel. Electroosmotic (EO) pumps (*a.k.a.* electrokinetic pumps) have no moving parts and are capable of generating high flow rate per device volume. People use electroosmotic pumping to achieve both significant flow rates and pressures, and a fairly wide range of working electrolytes may be used (including deionized water, buffered aqueous electrolytes). These devices have significant pressure capacity in a compact structure. We have achieved flow rates in excess of 400 micron/second. EO pumps offer some advantages over other miniature pumps for microchannel cooling applications and integrated bio-analytical systems.

High-pressure capacity, millimeter-scale, porous-media based EO pumps have been demonstrated [32, 33], and most of the micropumps which are presented in the literature are DCEO micropumps. However, DCEO micropump suffers from high voltage operation (several kVs) and consequently excessive electrochemical reactions and electrolysis at the electrodes. This high voltage operation also creates the pH gradients and bubble which is not favorable for micropumping [28-32]. Again, many of the current fabrication techniques of porous-media EO pumps are not compatible with standard microfabrication processes

and this poses a significant obstacle to the chip-level integration of EO pumps into microsystems. Our developed micropump is operated with smaller AC voltage and microfabrication compatible.
Reliability, compatibility, and cost are also criterions for selecting or designing micropumps. Micropumps must perform proposed functions without being damaged (re-usable), and at the same time must not bring changes in the medium. Compatibility with microsystems requires precisely pumping the desired range of fluid volumes and proper overall size of the micropump. Micropump can be used to manipulate the fluid volumes ranging from a few picoleters to hundreds of microliters for different biomedical applications, such as single molecule detection, species separation, antigen-antibody binding. The pump size is important for integrating the compact microsystem. The simplicity in design and fabrication of micropumps is also desirable. By using our fabricated micro-electrode array the problems of the electrokinetic micropumps can be solved.

4.1 The features of AC electroosmosis micropumps

Novel pumps based on ac electroosmosis are also investigated in this research. Here the AC electroosmosis is the main mechanism to drive fluids, which are quantitatively investigated by both experiments and Comsol simulations. Compared to other micropumps without moving parts, this AC electroosmotic micropump has following unique features.

1. Low operating voltage makes it superior in terms of device portability. In our design the AC electric fields are applied to pump fluids as small as 500mV bias voltage.
2. Avoids electrolysis and the resulting bubble generation. Currently EHD and MHD micropumps use DC fields to produce fluid motion, generating bubbles at the electrodes. In this research the applied AC fields has a frequency range of 100Hz to 5 KHz, allowing no time for bubble generation.
3. The dimension of our micropump is 5 mm long, 500 μm wide and 100 μm height. These pumps can be scaled down linearly to submicron/nanoscale or up by expanding laterally.
4. Minimizes pH gradient for using the smaller voltage.
5. The designed micropump is simple in structure. The channel and electrodes array are combined to achieve electroosmotic pumping. The designed ACEO micropump can also be integrated with lab-on-a-chip for miniaturization.

These features of the AC electroosmotic pump provide higher reliability, higher compatibility and lower cost. It can be possible for mass production of the electrode array on the wafer. The channel can also be fabricated using PDMS by using Si mold.
The designed AC electroosmotic pumps do not require open channels and hence are very useful for a sealed lab-on-a-chip system, where the fluid is circulating in closed channels. The use of this type of AC electroosmotic pump does not need open reservoir, avoiding undesired pressure due to different fluid heights in the reservoir.

4.2 Design of AC electroosmotic micropumps

Electroosmotic micropumps have been used widely in broad applications [33, 34]. Novel micropumps based on ACEO have been designed to drive fluids. AC electroosmotic micropumps can operate at lower voltage to avoid undesirable electrolysis and pH gradients. The main concept of getting the pumping action is to get the uni-directional flow by breaking the reflection-symmetry in the geometry or applied signal. Figure 9 shows the

pumping action breaking the symmetry by changing the geometry [35]. By using the asymmetric pattern of electrode bigger vortices are generated on the larger electrode, which eventually dominants and produce uni-directional flow. The smaller electrode still produces the counter-rotating vortices that reduce the net flow.

Our design of AC electroosmotic micropump is based on the biased AC electroosmosis technique for symmetrical electrode array. The separation of the in-pair symmetrical electrodes (80 micron size) are 40 μm. We repeated the pair of electrodes to make the array of electrodes. The separation of the elctrode pair is 100 μm. For this particular configuration we name it 80/40/100 configuration. The corresponding numerical simulations using the finite element software FEMLAB are also conducted to verify the concept. The good agreement between the simulations and the experimental data regarding the uni-directional flow is also demonstrated.

4.2.1 Capacitive and faradaic charging effect

Biased ACEO is realized by applying biased AC signals over electrode pairs, leaving the electrolyte floating; therefore, two electrodes have different electrical potentials relative to the electrolyte. With a biased AC signal, $V_{applied}=V_0(1+\cos\omega t)$ over the electrodes, the left electrode is always positive and more prone to Faradaic charging, while the other is always negative and subject to capacitive charging. For the biased signal one electrode has a positive offset with the potential always greater than zero, while the other one lower than zero (Fig. 9). When the voltage exceeds the threshold for reaction, asymmetric vortices are formed above two electrodes as faradaic reactions take place at the positively biased electrodes. Faradaic reaction generates co-ions following Faraday's law. For the other electrode with a negative offset, counter ions are attracted to the electrode. Therefore, for two electrodes, same polarity of ions is induced. A unidirectional fluid loop is consequently formed by tangential fields, as shown in Figure 9. For the negative particles in an aqueous environment, they adhere to the stagnation line on the positively biased electrode. Henceforward, biased ACEO exhibits directional particle assembly.

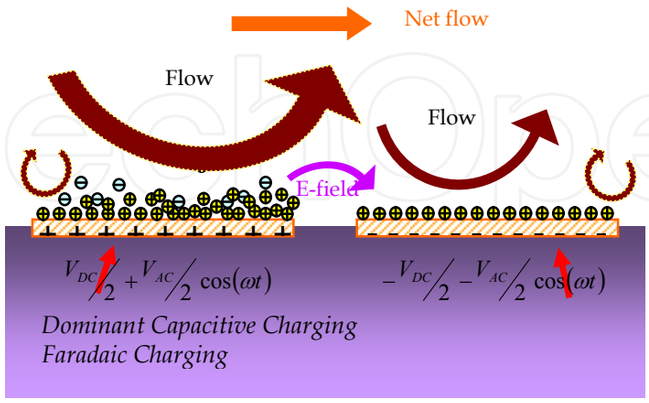

Fig. 9. Asymmetric polarization with appropriate magnitude can produce uni-directional micropumping.

Because most bioparticles are negatively charged, the DC bias can provide a synergy of AC and DC electrokinetics for more efficient particle collection. Electrophoretic/electrostatic

force is exerted simultaneously with ACEO to move bioparticles towards positively-biased electrodes, as shown in Figure 9. Figure 9 already explained the electric field direction and net fluid flow for the asymmetric biased electrode pattern. Also in next section we have experimentally proved unidirectional particle flow. Breaking the charging symmetry on electrodes are main concept of producing uni-directional flow. With the biased AC signal, one electrode is at a higher voltage and hence undergoes Faradaic charging with cations, and the other electrode is at a lower voltage and hence is polarized by capacitive charging with the cations as well. This combination of the two polarization on the two electrodes of an electrode pair produces a uni-directional flow on each of the electrode pairs on electrode array. Which eventually produce a continuation of fluid flow and show the pumping action.

4.2.2 Unidirectional ACEO micropump

When using the asymmetric electrode pattern the direction of the pumping can not be reversed. For several biomedical applications there is a need for bi-directional flow directions. A common medical treatment procedure makes the use of a bidirectional flow control of one or more fluids to and from a patient. For these applications we have developed the biased AC electroosmotic micropump which can operate in both directions. Here we have broken the symmetry by applying asymmetric voltage on the symmetric electrode pattern, which eventually breaks the symmetry of the pattern. Figure 10 shows the electrode array, where L_{pair} is the separation between the two electrode pairs and L_{array} is the separation within the electrode pair. The mechanism of the designed pump is explained in Fig 10. As shown in the picture, both positive biased electrode (faradic charging) and the negative biased electrode (capacitive charging) generate the same positive charges on the electrode. The electrode surface has an excess of positive charges that creates a uni-directional flow in electrode pair, which eventually produce net flow on the array of electrodes. However, the coupling between neighboring electrode pairs will produce counterflows to the net flow produced within the pair and reduce the pumping efficiency. To reduce the undesirable coupling between the two adjacent pairs, L_{array} is kept larger than L_{pair}, but not so large that the flow loses its momentum.

Figure 10 is the schematic of pumping action for symmetrical electrode pattern with the biased applied voltage. The spacing Lpair and Larray will be the controlling factor for the pumping velocity. The rule of thumb is $L_{array} > L_{pair}$, so that the consecutive electrodes of Lpair and Larray do not form the EO flow in the reverse direction. From our earlier experiment we already have got L_{pair} of 20μm for the 80/20 configuration of our electrode pattern, which produces the highest fluid velocity.

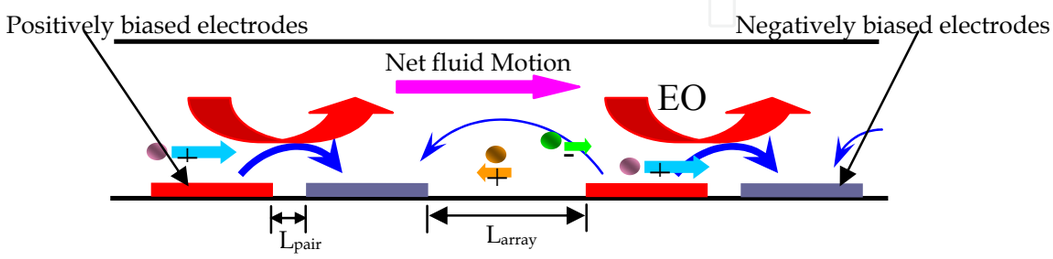

Fig. 10. Biased ACEO can produce uni-direction fuid motion, which also imparts differential velocities to particles with various charge/mass ratio.

Biased ACEO pump will be investigated by manipulating the faradic charging effect. We will also study the improvement in the pumping velocity. The pumping setup is shown in figure 11. The channel dimension is 350µm X 1.5mm X 5mm. The highest measured velocity for this pump is 150 µm/sec.

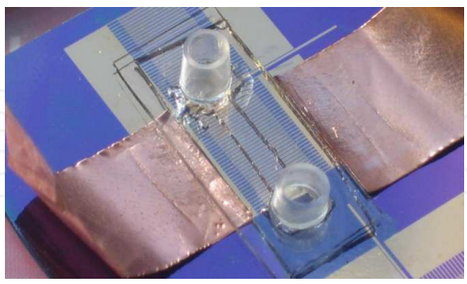

Fig. 11. Experimental setup of first version of the micropump.

4.3 Experimental results

ACEO flow is examined using microfabricated arrays of electrode pairs on silicon substrate. Au/Cr (90nm/10nm thickness) electrodes were fabricated by lift-off procedure in IC processing. Cr is the adhesion layer between the substrate and Au, and Au is in contact with electrolytes. The electrodes were 20 mm long, 0.1 µm think, 80 µm wide with a 20 µm separation (denoted as 80/20). Microfluidic chambers were formed by sealing silicone microchambers (PC8R-0.5, Grace Bio-Labs, Inc.) over the wafer, which have a height of 500 µm. Polystyrene spheres (1 µm diameter; Fluka Chemica) seeded in DI water was used to track fluid motion.

Figure 12 gives the comparative analysis of the microfluidic velocity generated using four types of patterned Au electrodes. The 80/20 configuration gives the highest velocity, which is suitable for the pumping application.

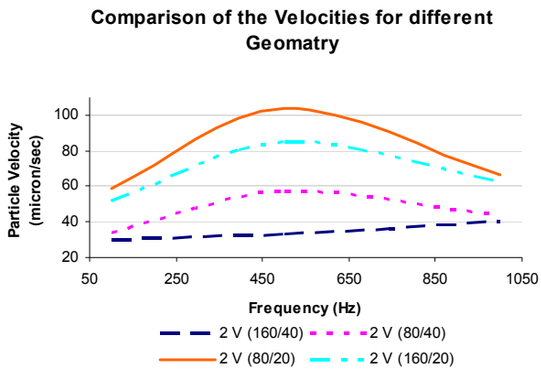

Fig. 12. Microfluidic Experiment result & comparison of four types of electrode geometry

4.4 Optimization of biased ACEO micropump

The goal of the research is to minimize the micropump reverse flow velocity. Obviously we increase the applied voltage it will increase the pumping velocity, and it will also increase the reverse pumping velocity (for the vortices). So, here we have focused on decreasing the

reverse direction flow. Figure 13 explains the optimization concept by decreasing the channel height of the microfluidic chamber. Later on we also have presented the numerical simulation using Comsol Multiphysics for three different channel heights and verified the concept. The experimental result demonstrates that the thinner channel height ~ 100 μm increases the velocity of the micropump. In this case we also have demonstrated the bulk fluid flow, as here the surface to volume ratio is high.

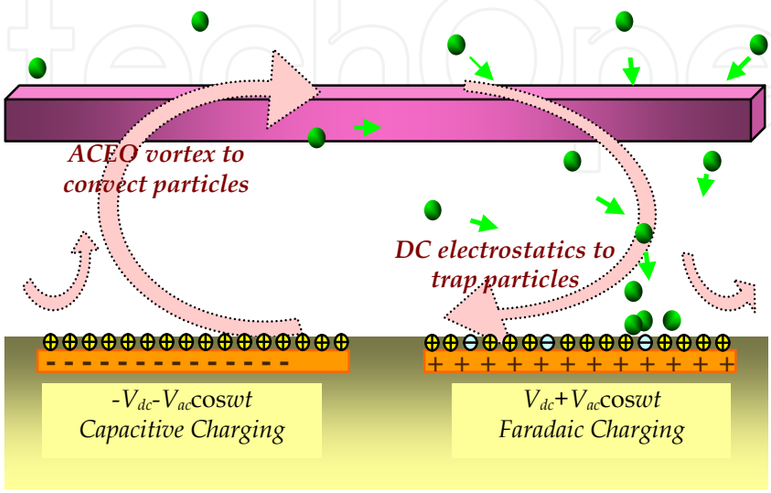

Fig. 13. Optimization Concept: to decrease the channel height to reduce the reverse flow

As seen from figure 13, the big vortex is suppressed / obstructed by the top wall of the channel. According to our analysis the vortex size is depended on the electrode geometry and the channel height. For the fixed electrode geometry the size of the vortex is only depended on the channel height, which is explained by Comsol Multiphysics simulation. The boundary condition for inflow and outflow was the key factor to run the simuation. Our findings show that smaller channel height will increase the surface flow, which will be described more in the next section.

Simulation of ACEO micropump has been performed prior to experiments. The simulation model, consists of two symmetrical electrodes of 80 μm width and the separation between the electrodes are 40 μm. The height of the chamber is 200 μm. From simulation we found that at the edge of the electrode the electric field is maximum. After simulating the electric field analysis the Navier-Stokes simulation is done to calculate the velocity field in the chamber. Initial fluid velocity is set to zero for the Navier-Stokes (NS) simulation. The fluid motions are generated by applied electric signals and a large vortex is formed for biased applied signal.

5. ACEO sensor integrated with microcantilever

We have investigated another microstructural design for ACEO devices, which is similar to a pair of parallel plates (Fig. 15). In this configuration, electrodes are facing each other, similar to a pair of parallel plates. The two face-to-face electrodes are asymmetric in design, so they produce non-uniform electric field. For mechanism identical to that of planar electrodes, surface EO flows are generated from the electrode edges inwards, and slow down to stagnation at the center, where particles are expected to trap.

5.1 ACEO particle trap

ACEO can transport the particles from a large region in the bulk fluid to the electrode surface. The flow velocity is important for optimizing the micropump and particle transportation. In contrast to electrophoretic and dielectrophoretic (DEP) velocity, which are typically limited to less than 20 microns per second [9], the ACEO velocity exceed 100 micron/sec. Figure 14(a) shows the initial distribution of particles when no signals are applied over the electrodes. Figure 14(b) shows that particles accumulated from both sides into lines at approximately $1/\sqrt{2}$ of electrode width [12]. This corroborates the theoretic prediction, since fluid velocity reduces at the null points of electric fields, and particles become trapped to the electrodes due to surface forces of between particles and electrodes.

For the biased ACEO experiments, applied voltage exceeds the threshold for reactions at V0=1.5V (i.e. high level & low level of biased voltage is 3V & 0V respectively). At the same voltage, the maximum flow velocity shifts to higher frequency compared with symmetric AC signals. This is because Faradaic polarization becomes suppressed at high frequency. Beyond 500Hz, microflows from capacitive charging are much stronger than those from Faradaic charging, so that the stagnation point on the left electrode disappears. At 100Hz, streamlines from capacitive charging and Faradaic charging become connected, forming a large vortex over the electrode pair and the particles aligned on the right electrode. Figure 14b also validates the null point formation by Comsol Multiphysics simulation in Figure5.

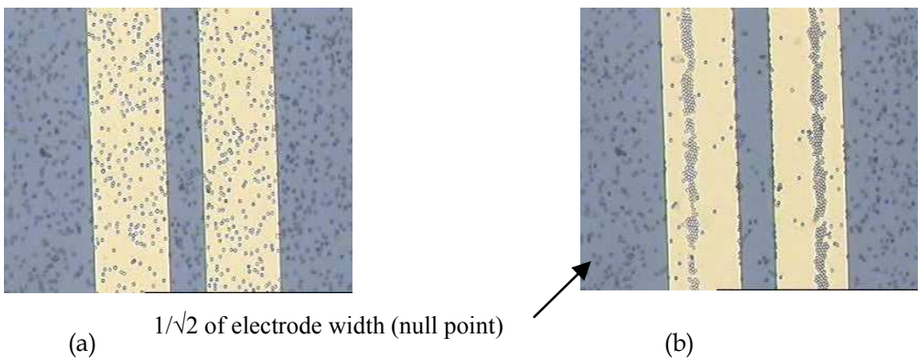

Fig. 14. (a) Particle without the supply voltage (b) Experimental picture of the particles accumulating at the 1/√2 electrode width;

5.2 Electric field analysis of parallel plate particle trap

Most ACEO devices reported so far adopt a side-by-side (interdigitated) configuration. To integrate such design on microcantilevers would call for sophisticated microfabrication. We use a face-to-face configuration, very much like a pair of parallel plates, with one plate having smaller electrode area than the other, as shown in Figure 15. As the top and bottom electrodes are asymmetric, the tangential electric fields are generated which induces electro-osmotic fluid motion. For the first half cycle as in Figure 15a, the bottom electrode is at positive potential, and negative ions are induced at the interface of the electrode and fluid. These negative ions interact with the electric field and produce two counter-rotating vortices from electrode edges inward on the electrode surface, creating null point at the center of the electrode.

Fig. 15. Concept of Parallel plate particle trapping for an AC cycle; (a) during the half cycle when the bottom electrode has positive polarity and ITO coated top electrode is negative; (b) next half cycle with opposite polarity. Flow motion and induced charges is also shown

For the next half cycle as in Figure 15b, applied potentials switches polarity and the bottom electrode is at negative potential. Here the induced positive ions will interact with the electric field and again produces two counter-rotating vortices from electrode edges inward, and fluid motions are sustained thus the particles are trapped at the centre of the electrode. As the bottom plate is smaller than the top plate, the electric field is almost always normal to the top electrode, hence tangential force can be neglected.

The tangential electric field for the asymmetric electrode pattern induces electro-osmotic fluid motion in the bottom plate. It is the microfluidic flow that conveys particles from the bulk of the fluid onto the fluid surface. The stagnation point created at the centre of the bottom plate. The particles are trapped at the stagnation point of the fluid.

5.3 Microcantilever particle trapping using ACEO

This section explains the novel particle trapping method using microcantilever. Here we have presented the first integration of the microcantilever with the ACEO particle trapping mechanism. Recently microcantilever sensor technology has boomed and become a promising sensor technology. Microcantilever sensors have several advantages over many other sensor technologies, including faster response time, lower cost of fabrication, the ability to explore microenvironments, and improved portability. Cantilever resonance responses, such as frequency, deflection, Q-factor, and amplitude, undergo changes due to adsorption or changes in environment. Resonance frequency of a microcantilever can be used to detect particles. When the target is loaded on the microcantilever, the resonance frequency of microcantilever is going to change. That means for the mass loading on the cantilever the resonance frequency is supposed to go down.

The parallel plate design has been used to attract particles onto cantilevers for high sensitivity detection [14]. Because particle trapping/concentrating effect is more obvious with the smaller electrode, in our design the metal-coated cantilevers are facing one large electrode (covering a whole fluid chamber), so that particles will aggregate on the cantilevers. The tangential electric field of parallel plate configuration is generated for the asymmetric electrode pattern, which induces electro-osmosis fluid motion. In our design of microcantilever trap, the metal-coated cantilevers substitute the patterned bottom electrode, so that particles will aggregate on the cantilevers [15]. Figure 16 shows the experimental setup of cantilever particle trap.

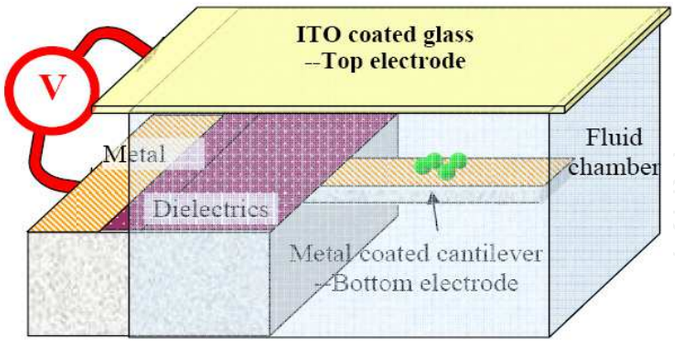

Fig. 16. Experimental Setup of Cantilever particle trap

As shown in Figure 16, photoresists (dielectrics) are coated on the conductive areas other than the cantilevers to suppress unwanted local EO flows. The ITO glass slide works as the top electrode, which is covering the whole fluid chamber. We have used Au-coated AFM probes as the MC, which has the dimension of 125μm X 30μm X 4μm. Tipped MC side was not used to avoid sharp electric fields.

Figure 17 shows the experimental results of trapping 200nm fluorescent particles on MC. After applying the AC signal (100Hz, 400mVp-p), suspended particles accumulate at the center of the cantilever from all directions. As time passes, more fluorescent particles from the surrounding area accumulated and formed bright object pattern. After the particle trapping on the surface, the MC was dried with AC signals applied, so that particles will not get dispersed by diffusion, surface tension, etc. Then the particle trapping effect was verified with AFM resonance measurement.

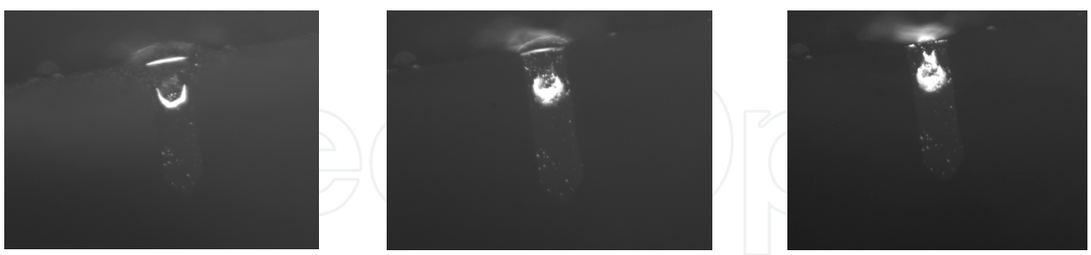

(a) (b) (c)

Fig. 17. Image sequence of 200 nm fluorescent particles trapped on the micro-cantilever;

5.3.1 Microcantilever particle trapping validation

To verify the concentrated particle trapping on MC, we also measure the resonance frequency of MC before and after trapping experiments. MC resonance frequency is inversely proportional to the differential mass of cantilever [21]. The sensitivity of a cantilever to mass loading is mainly determined by the excited cantilever resonance frequency.

$$\Delta m = \frac{K}{4\pi^2}\left(\frac{1}{f'^2} - \frac{1}{f^2}\right)$$

Where, Δm is the mass change;
K=sensor spring constant;
f = resonance frequency before mass adsorption;
And f' is the resonance frequency during mass adsorption.

Changes in the mass and surface properties of the microcantilever through binding or hybridization of analytes to receptor molecules will directly influence its surface stress. This causes the microcantilever to deflect and the deflection is proportional to the analyte concentration and inversely proportional to mass loading. The more the particle concentration on ACEO-cantilever, the more is the bending. So the more mass on the cantilever means the lower resonance frequency. From our experimental result (Fig. 18) we have got the resonance frequency of the MC goes down to 276.07 KHz after particle trapped on the MC for ACEO, which translates to a change of mass. For a change in mass we get,

$$\frac{f_1}{f_2} = \frac{\sqrt{m_{eff} + \Delta m}}{\sqrt{m_{eff}}}$$

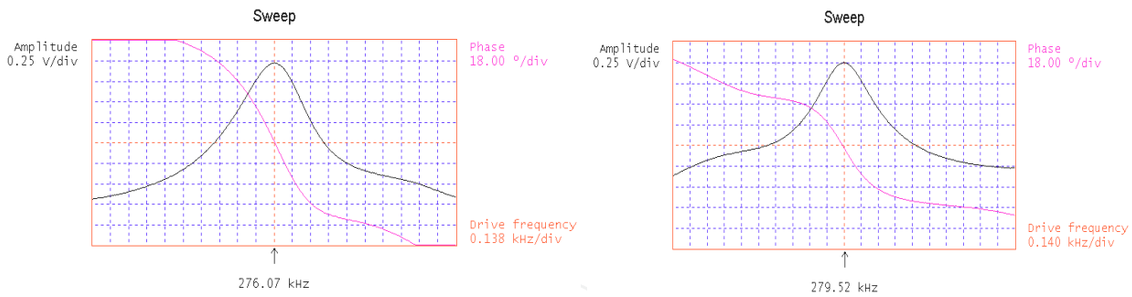

(a) (b)

Fig. 18. Resonance frequencies of the MCs (measured with multimode AFM.)
(a) After the particle trapping by ACEO, 276.07 kHz, (b) Control experiment with no electric signal applied, 279.52 kHz.

Microcantilever dimension is 125μm x 30μm x 4μm. The volume of the MC is 1.5e-14 m^3. Microcantilever is Si based, and the density of Si is 2330 kg/m^3. So the mass of microcantilever is 3.495e-8 gm. By putting the frequency and mass values in equation (4.2), we have got an increase of 2.52% increase of mass for the frequency change from 279.52 KHz to 276.07 KHz. The change in resonant frequency as a function of the particle mass binding on the cantilever beam surface forms the basis of the particle detection scheme.

5.3.2 Analysis of particle trapping using SEM

Our research also shows that applying the electric field creates a certain crystal shape of the concentrated particles. Without applying the electric field, the particles are accumulating in layers, and formed no crystal shape (Fig. 19a). But when the electric field was applied for ACEO, the particles formed the close-packed layer of colloidal particles, and take the shape of crystalline structure, as shown in Figure 19(b). Compare with the Figure 19(a), the crystalline structure (Fig. 19b) increases the number of particles in the bottom layer [22].

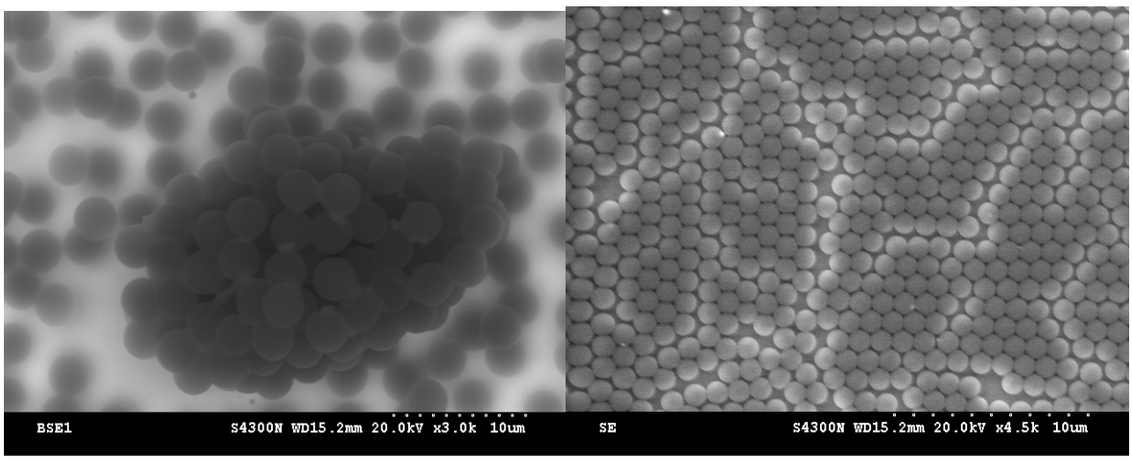

(a) (b)

Fig. 19. SEM image of the particles; (a) Particles dried on the surface, no electric field is applied (b) For ACEO particle trapping, particles take the Crystal Shape.

6. Conclusion

AC electroosmosis, with its advantages of low power, low voltage and higher velocity, has been used to develop pumps. Such AC electrokinetic micropumps are presented in literature which have fast pumping (velocities » mm/s) velocity with low driving voltage of a few volts. But the literature review used the asymmetric pattern of electrodes. This chapter presents the novel micropump which utilizes the symmetric electrode pattern with the bias AC voltage. The chapter also focused on the MEMS microcantilever integration with ACEO.

The novel DC-biased, AC electroosmotic micropump operates in low voltage to avoid undesirable electrolysis and pH gradients. The developed uni-directional micropump prototype breaks the symmetry of the electrode array by applying the DC-biased AC signal, which has proven to be advantageous when compared to those pumps that use only asymmetric electrode patterning. In this work, a novel technique also has been developed to

trap the particles and pump the fluid. Interfacing the micro-cantilever with ACEO mechanism has expanded its capability for biological, physical and chemical detection and makes the whole system ultra sensitive. The research work substantially enriches the portfolio of transducers, lab-on-a-chip (LOC) and MEMS that can be used in high performance miniaturized analytical systems.

7. Acknowledgment

This work is supported in part by the Nanotechnology for Undergraduate Education Program of the National Science Foundation (NSF-NUE) under Award Number EEC-1138205. The work is also supported from the internal fellowship grant from the University of Texas at Brownsville. We also want to thank Arizona State University (ASU) Nanofab Laboratory for assistance with microfabrication.

8. References

[1] Helene Andersson, Albert ven den Berg, " Microfluidic devices for cellomics : A review", Sensors and Actuators, B 92, (2003), 315-325.

[2] Vincent Studer, Anne Pépin, Yong Chen, and Armand Ajdari, "An integrated ac electrokinetic pump in a microfluidic loop for fast and tunable flow control", Analyst, vol. 129, pp. 944-949, 2004.

[3] C.-H. Chen and J.G. Santiago, "A planar electroosmotic micropump," J. Microelectromech. Syst., vol. 11, pp. 672-683, 2002.

[4] Lastochkin, D., Zhou, R., Wang, P., Ben, Y. and Chang, H.-C., "Electrokinetic Micropump and Micromixer Design Based on AC Faradaic Polarization", J. of Applied Physics , 96 , 1730 (2004).

[5] K. H. Bhatt, S. Grego and O. D. Velev, "An AC Electrokinetic Technique for Collection and Concentration of Particles and Cells on Patterned Electrodes," *Langmuir* 21, pp. 6603-6612, 2005.

[6] M. R. Brown, and C. D. Meinhart, "AC electroosmotic flow in a DNA concentrator," Microfluidics & Nanofluidics, ISSN:1613-4982 (Print) 1613-4990 (Online), 2006.

[7] Ronald F. Probstein, Physicochemical Hydrodynamics : An Introduction, 2nd Editon, New York : John Wiley and Sons, c 1994

[8] Stone, H.A. and S. Kim, "Microfluidics: Basic issues, applications, and challenges," AIChE J., 47(6), 1250-1253 (2001).

[9] A. Ramos, H. Morgan, N. G. Green and A. Castellanos, "AC electrokinetics: a review of forces in microelectrode structures", J. Phys. D: Appl. Phys. 31(1998) 2338–53

[10] A. Ramos, H. Morgan, N. G. Green and A. Castellanos, "AC electric-field-induced fluid flow in microelectrodes", J. Colloid Interface Sci. 217(1999) 420–2

[11] J. Wu, "Electrokinetic Microfluidics for On-Chip Bioparticle Processing," IEEE Trans. Nanotech., Mar. 2006.

[12] J. Wu, Y. Ben and H.-C. Chang, "Particle Detection by Micro- Electrical Impedance Spectroscopy with Asymmetric-Polarization AC Electroosmotic Trapping," Microfluidics & Nanofluidics, 1(2), pp. 161-167, 2005

[13] Julio M. Ottino and Stephen Wiggins, " Introduction: mixing in microfluidics", Phil. Trans. Royal Society Lond. A (2004) 362, 923-935.

[14] N. Islam, M. Lian, S. Swaminathan and J. Wu, "Micro/Nano- Particulate Fluid Manipulation in AC Electro-Kinetic Lab-on-a-Chip," 2nd ASM - IEEE EMBS Conf. Bio, Micro & Nanosyst., Jan. 15-18, 2006, San Francisco, CA, USA.

[15] J. Wu, N. Islam and M. Lian, "High Sensitivity Particle Detection By Biased AC Electro-Osmotic Trapping on Cantilever," 19th IEEE Int'l Conf. Micro Electro Mechanical Systems (MEMS 2006), Jan. 22-26, 2006, pp. 566 – 569, Istanbul, Turkey.

[16] N. Islam, M Lian, and J. Wu, "Enhancing Microcantilever Sensitivity with Integrated AC Electroosmotic Trapping," submitted to Bio-microfluidics Journal.

[17] J. Wu and H.-C. Chang, "Asymmetrically Biased AC Electrochemical Micropump," AIChE annual meeting 2004, Nov. 7 – 12, Austin, TX.

[18] Rosenthal A, Voldman J, "Dielectrophoretic traps for single-particle patterning," Biophysical Journal, 88(3), pp. 2193-2205, 2005.

[19] Meinhart C D, Wang D and Turner K, "Measurement of AC Electrokinetic Flows," J. Biomedical Microdevices, 5(2), 139-145, 2003

[20] Morgan H, Green N G, "Electrokinetics: Colloids and Nanoparticles," Research Studies Press Ltd: UK 2002

[21] Sepaniak M, Datskos P, Lavrik N, Tipple C, "Microcantilever Transducers: A New Approach in Sensor Technology," Analytical Chemistry, November 1, pp. 568A-575A, 2002.

[22] Green N G, Ramos A, Gonzalez A, Morgan H, and Castellanos A, "Fluid flow induced by nonuniform ac electric fields in electrolytes on microelectrodes. III. Observation of streamlines and numerical simulation," Physical Review E 66, 026305, 2002.

[23] Taylor, M. T., " Simulation of microfluidic pumping in a genomic DNA blood-processing cassette," Journal of Micromechanics and Microengineering, 2003. 13(2): pp 201-208.

[24] Laser, D. and J. Santiago, "A Review of micropumps," J. Micromechanics and Microengineering, 2004. 14:pp R34-R64.

[25] T.M. Squires and M.Z. Bazant, "Induced-charge Electro-osmosis," J. Fluid Mech., 509, pp. 217-252, 2004.

[26] Vincent Studer, Anne Pépin, Yong Chen, and Armand Ajdari, "An integrated ac electrokinetic pump in a microfluidic loop for fast and tunable flow control", The Analyst Journal, 129, 944-949, 2004.

[27] J. Wu, N. Islam and M. Lian, "High Sensitivity Particle Detection By Biased AC Electro-Osmotic Trapping on Cantilever," 19th IEEE Int'l Conf. Micro Electro Mechanical Systems (MEMS 2006), Jan. 22-26, 2006, pp. 566 – 569, Istanbul, Turkey.

[28] M. Z. Bazant, T. M. Squires, "Induced-charge Electrokinetic Phenomena: Theory and Microfluidic Applications", Phys. Rev. Letter, 92(6), 066101 (2004)

[29] A. Castellanos, A. Ramos, A. Gonzalez, N. G. Green, and H. Morgan, "Electrohydrodynamics and dielectrophoresis in microsystems: Scaling laws," J. Phys. D, Appl. Phys., vol. 36, pp. 2584–2597, 2003.

[30] Josh H. M. Lam, Raymond H. W. Lam, Kin Fong Lei, Winnie W. Y. Chow and Wen J. Li, "A Polymer-based Micro fluidic Mixing System Driven by Vortex Micropumps", Proceedings of the 5th World Congress on Intelligent Control and Automation, June 15-19, 2004.

[31] C. Liu, D. Cui, H. Cai, X. Chen, Z. Geng, "A rigid poly(dimethylsiloxane) sandwich electrophoresis microchip based on thin-casting method", Electrophoresis 2006, 27, 2917–2923

[32] N.G. Green, A. Ramos, A. Gonzalez, A. Castellanos, and H. Morgan, "Electrothermally induced fluid flow on microelectrodes," Journal of Electrostatics, 53 (2001) 71-87.

[33] Lastochkin, D., Zhou, R., Wang, P., Ben, Y. and Chang, H.-C., "Electrokinetic Micropump and Micromixer Design Based on AC Faradaic Polarization", J. of Applied Physics , 96 , 1730 (2004).

[34] Iki, N., H. Hoshino, and T. Yotsuyanagi, " A capillary electrophoretic reactor with an electroosmosis control method for measurement of dissociation kinetics of metal complexes," Analytical Chemistry, 2000. 72(20): pp. 4812-4820.

[35] A. Ramos, A. Gonzalez, A. Castellanos, N.G. Green, and H. Morgan, "Pumping of liquids with ac voltages applied to asymmetric pairs of microelectrodes," Phys. Rev. E, 67, 056302 (2003).

[36] Shaorong Liu, Qiaosheng Pu, and Joann J. Lu, "Electric field-decoupled electroosmotic pump for microfluidic devices", Journal of Chromatography A, 1013 (2003), 57-64.

[37] Ping Wang, Zilin Chen, and Hsueh-Chia Chang, "A new electro-osmotic pump based on silica monoliths", ELSEVIER-Sensors and Actuators B113 (2006), 500-509.

[38] A. Ramos, H. Morgan, N. G. Green, A. Castellanos. "AC electrokinetics: a review of forces in microelectrode structures". J. Phys. D: Appl. Phys. Vol 31. pp 2338-2353.

[39] N.G. Green, A. Ramos, A. Gonzalez, H. Morgan, and A. Castellanos, "Fluid flow induced by nonuniform ac electric fields in electrolytes on microelectrodes. III. Observation of streamlines and numerical simulation," Physical Review E, 2002, Vol.66, 026305

[40] Shuhuai Yao and Juan G. Santiago, "Porous glass electroosmotic pumps: theory", ELSEVIER- Journal of Colloid and Interface Science, 268 (2003), 133-142.

[41] Chuan-Hua Chen and Juan G. Santiago, "A Planar Electroosmotic Micropump", Journal of Microelectromechanical Systems, Vol.11, No.6, December 2002.

[42] P. H. Paul, D.W. Arnold, and D. J. Rakestraw, "Electrokinetic generation of high pressures using porous microstructures," in _-TAS 98, Banff, Canada, 1998.

[43] S. Zeng, C. H. Chen, J. C. Mikkelsen Jr., and J. G. Santiago, "Fabrication and characterization of electroosmotic micropumps," Sensors Actuat. B, vol. 79, pp. 107–114, 2001

[44] A. Ramos, A. Gonzalez, A. Castellanos, N.G. Green, and H. Morgan, "Pumping of liquids with ac voltages applied to asymmetric pairs of microelectrodes," Phys. Rev. E, 67, 056302 (2003).

[45] N. Islam and J. Wu, "Microfluidic Transport by AC Electroosmosis", Journal of Physics: Conference Series, 34, pp. 356 – 361, 2006s

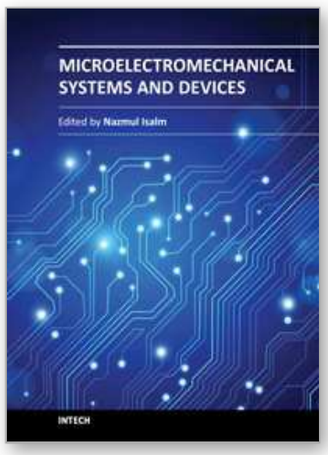

Microelectromechanical Systems and Devices

Edited by Dr Nazmul Islam

ISBN 978-953-51-0306-6
Hard cover, 480 pages
Publisher InTech
Published online 28, March, 2012
Published in print edition March, 2012

The advances of microelectromechanical systems (MEMS) and devices have been instrumental in the demonstration of new devices and applications, and even in the creation of new fields of research and development: bioMEMS, actuators, microfluidic devices, RF and optical MEMS. Experience indicates a need for MEMS book covering these materials as well as the most important process steps in bulk micro-machining and modeling. We are very pleased to present this book that contains 18 chapters, written by the experts in the field of MEMS. These chapters are groups into four broad sections of BioMEMS Devices, MEMS characterization and micromachining, RF and Optical MEMS, and MEMS based Actuators. The book starts with the emerging field of bioMEMS, including MEMS coil for retinal prostheses, DNA extraction by micro/bio-fluidics devices and acoustic biosensors. MEMS characterization, micromachining, macromodels, RF and Optical MEMS switches are discussed in next sections. The book concludes with the emphasis on MEMS based actuators.

INTECH
open science | open minds

InTech Europe
University Campus STeP Ri
Slavka Krautzeka 83/A
51000 Rijeka, Croatia
Phone: +385 (51) 770 447
Fax: +385 (51) 686 166
www.intechopen.com

InTech China
Unit 405, Office Block, Hotel Equatorial Shanghai
No.65, Yan An Road (West), Shanghai, 200040, China
中国上海市延安西路65号上海国际贵都大饭店办公楼405单元
Phone: +86-21-62489820
Fax: +86-21-62489821

IntechOpen